A Letters Journal Exploring the Frontiers of Physics

September 2023

EPL, **143** (2023) 66001
doi: 10.1209/0295-5075/acf59e

www.epljournal.org

Perspective

Tunneling time and Faraday/Kerr effects in $\mathcal{PT}$-symmetric systems

Vladimir Gasparian[1], Peng Guo[1,2,3(a)], Antonio Pérez-Garrido[4] and Esther Jódar[4]

[1] *Department of Physics and Engineering, California State University - Bakersfield, CA 93311, USA*
[2] *College of Arts and Sciences, Dakota State University - Madison, SD 57042, USA*
[3] *Kavli Institute for Theoretical Physics, University of California - Santa Barbara, CA 93106, USA*
[4] *Departamento de Física Aplicada. Hospital de Marina, Universidad Politécnica de Cartagena (UPCT) 30202 Cartagena, Murcia, Spain*

received 24 August 2023; accepted in final form 31 August 2023
published online 22 September 2023

Abstract – We review the generalization of tunneling time and anomalous behaviour of Faraday and Kerr rotation angles in parity and time ($\mathcal{PT}$)-symmetric systems. Similarities of two phenomena are discussed, both exhibit a phase transition-like anomalous behaviour in a certain range of model parameters. Anomalous behaviour of tunneling time and Faraday/Kerr angles in $\mathcal{PT}$-symmetric systems is caused by the motion of poles of scattering amplitudes in the energy/frequency complex plane.

Introduction. – During the past two decades, parity-time ($\mathcal{PT}$)-symmetric Hamiltonians are studied in various areas of physics such as optics [1–5], quantum mechanics [6–8], and classical wave systems [9,10]. For example, in optics, $\mathcal{PT}$-symmetric arrangements of gain and loss media have been studied, where the gain balances the loss, leading to interesting phenomena such as unidirectional invisibility and anomalous point oscillations [11,12]. Note that although $\mathcal{PT}$-symmetric systems have been extensively studied and have theoretical and experimental support, their implementation in certain physical systems can still be difficult. Nevertheless, they remain an active research field with great potential for new discoveries and technical applications in optical isolators, sensors, magnetic storage, magneto-optical modulators, magneto-optical switches, and magneto-optical circulators.

In this letter, we present a brief review on i) the generalization of the concept of tunneling time in $\mathcal{PT}$-symmetric systems and ii) some anomalous behaviours of magneto-optic effects in $\mathcal{PT}$-symmetric systems. Both quantum tunneling time and magneto-optic effects are the consequence of propagation of either quantum wave or optical wave through barriers, hence both phenomena are closely related to the transmission and reflection amplitudes of scattering of a quantum particle or light off barriers, and can be described in a similar framework.

In standard (Hermitian) quantum mechanics, both tunneling time of a quantum particle and Faraday and Kerr rotations of an electromagnetic wave through real potential barriers are not new subjects, and a wide variety of theoretical and experimental work on both topics has been carried out extensively in the past:

i) Tunneling time: Substantial research has been conducted on the tunneling time problem, see, *e.g.*, refs. [13–15] and references therein). This area of exploration is particularly focused on nanostructures and mesoscopic systems with sizes smaller than 10 nm. In such systems, the tunneling time assumes significance as it becomes a key factor in determining various transport properties. Notably, it plays a vital role in phenomena such as the frequency-dependent conductivity response of mesoscopic conductors [16] and the occurrence of adiabatic charge transport [17,18]. More recently, another kind of problems have arisen in ultrafast science or in attosecond physics (*e.g.*, the investigation of electron correlation effects, photoemission delay, ionization tunneling, etc.), where tunneling time experiments play an important role as a unique and powerful tool that allows electronic monitoring with subatomic resolution both in space and time. The measurement of tunneling time in attosecond

(a) E-mail: peng.guo@dsu.edu (corresponding author)

experiments (attosecond $= 10^{-18}$ s) offers a fruitful opportunity to understand the role of time in quantum mechanics, which has been controversial since the appearance of quantum mechanics, see, *e.g.*, refs. [13,15,19].

ii) Magneto-optic effects: The development of electromagnetic theory and atomic physics has been largely influenced by the study of the magneto-optic effects as Faraday rotation (FR) and Kerr rotation (KR). In these magneto-optical phenomena, an electromagnetic wave propagates through a medium altered by the presence of an external magnetic field. In such magneto-optical materials (also referred as gyrotropic or gyromagnetic), left- and right-rotating elliptical polarizations propagating at different speeds result in a rotation of the planes of the transmitted (FR) and reflected (KR) light. FR and KR effects are essential for optical communication technologies [20], optical amplifiers [4,21], and photonic crystals [22,23]. In addition, the KR is also an extremely accurate and versatile research tool and can be used to determine quantities, such as anisotropy constants, exchange-coupling strengths and Curie temperatures (see, *e.g.*, [24]).

General theory of tunneling time and magneto-optic effects in $\mathcal{PT}$-symmetric systems. – A brief summary of general theory of tunneling time and magneto-optic effects in $\mathcal{PT}$-symmetric systems is given in this section, more details can be found in [25–28].

Tunneling time. The concept of tunneling or delay time for a quantum particle tunneling through real potential barriers is conventionally defined through the integrated density of states, which is proportional to the imaginary part of the full Green's function of systems and positive definite in a real potential scattering theory. Following the definition in refs. [29–31], two components of the traversal time τ_E can be introduced by ($\hbar = 1$)

$$\tau_E = \tau_2 + i\tau_1 = -\int_{-\frac{\Lambda}{2}}^{\frac{\Lambda}{2}} \mathrm{d}x \langle x|\hat{G}(E)|x\rangle, \tag{1}$$

where τ_1 and τ_2 represent Büttiker-Landauer tunneling time and the Landauer resistance, respectively. The Λ stands for the length of the potential barrier, and the $\hat{G}(E) = \frac{1}{E-\hat{H}}$ is the Green's function operator of the system. As shown in refs. [30,31], two components of the traversal time τ_E are linked to the scattering and transport amplitudes explicitly by

$$\tau_2 + i\tau_1 = \frac{\mathrm{d}\ln[t(k)]}{\mathrm{d}E} + \frac{r^{(l)}(k) + r^{(r)}(k)}{4E}, \tag{2}$$

where $t(k)$ and $r^{(l/r)}(k)$ are the transmission and left/right reflection amplitudes, respectively, and $k = \sqrt{2\,\mathrm{m}E}$ is the momentum of particle. The transmission and reflection amplitudes can be obtained by finding scattering solutions of the Schrödinger equation,

$$\hat{H}|\Psi_E\rangle = E|\Psi_E\rangle, \qquad \hat{H} = -\frac{1}{2\,\mathrm{m}}\frac{\mathrm{d}^2}{\mathrm{d}x^2} + V(x), \tag{3}$$

where m denotes the mass of the particle, and $V(x)$ is the interaction potential.

In the conventional real potential scattering theory, the development of the concept of tunneling or delay time is fundamentally based on counting the probability that a particle spends inside of a barrier, see, *e.g.*, refs. [32–34]. However, in complex potential scattering theory, the norm of states is no longer conserved, the probability interpretation of tunneling time becomes problematic. This can be understood by examining the spectral representation of Green's function in a complex potential scattering theory, which now depends on the eigenstates of both $\hat{H}$ and its adjoint $\hat{H}^\dagger$,

$$\hat{G}(E) = \sum_i \frac{|\Psi_{E_i}\rangle\langle\widetilde{\Psi}_{E_i}|}{E - E_i}, \tag{4}$$

where

$$\hat{H}^\dagger|\widetilde{\Psi}_E\rangle = E|\widetilde{\Psi}_E\rangle. \tag{5}$$

In general the discontinuity of Green's function crossing the branch cut in the complex E-plane is a complex function. However, see ref. [25], it is real under $\mathcal{PT}$ symmetry and equal to the imaginary part of the Green's function, though it may not always be positive as a consequence of the norm violation due to the complex potential. Hence, the conventional definition of density of states gets lost, and one should generalize and redefine correctly the tunneling time. In this review letter the tunneling time through $\mathcal{PT}$-symmetric barriers is defined by eq. (1). The generalized density of states in such a system is taken as the imaginary part of Green's function, and τ_1 now may be interpreted as a generalized Büttiker-Landauer tunneling time. The sign of generalized tunneling time τ_1 is directly related to the potential barriers, that either tend to keep a particle in or force it out. When τ_1 is negative it behaves similarly to a forbidden gap in a periodic system, being unreachable.

Magneto-optic effects. We consider an incident linearly polarized electromagnetic plane wave with an angular frequency ω entering the system from the left, propagating along the x-direction. The electric field's polarization direction of the incident wave is aligned with the z-axis: $\boldsymbol{E}_0(x) = e^{i\frac{\omega}{c}\sqrt{\epsilon_0}x}\hat{z}$, where ϵ_0 denotes the dielectric constant of vacuum. A magnetic field $\boldsymbol{B}$ is applied in the x-direction, as depicted in fig. 1. The scattering of the EM wave is described by, see, *e.g.*, refs. [35,36],

$$\left[\frac{\mathrm{d}^2}{\mathrm{d}x^2} + \frac{\omega^2\epsilon_\pm(x)}{c^2}\right] E_\pm(x) = 0, \tag{6}$$

where $E_\pm = E_y \pm iE_z$ represents the circularly polarized electric fields. The variable $\epsilon_\pm(x)$ is defined as follows:

$$\epsilon_\pm(x) = \begin{cases} \epsilon + V(x) \pm g, & \text{if } x \in \left[-\frac{L}{2}, \frac{L}{2}\right], \\ \epsilon_0, & \text{otherwise,} \end{cases} \tag{7}$$

where L represents the length of the dielectric slab and ϵ is the positive and real permittivity of the slab, see fig. 1.

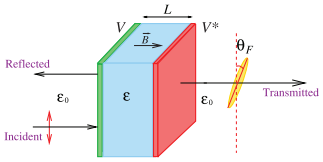

Fig. 1: Demo plot of a $\mathcal{PT}$-symmetric dielectric slab model with two balanced complex narrow slabs placed at both ends of a real dielectric slab.

$V(x)$ denotes the additional potential barriers that are placed inside of the slab, which can be easily manipulated and adjusted to implement the $\mathcal{PT}$ symmetry requirement. g is the gyrotropic vector along the magnetic-field direction. The external magnetic field $\boldsymbol{B}$ is included into the gyrotropic vector g to make the calculations valid for the cases of both external magnetic fields and magneto-optic materials. The magnetic field causes the direction of linear polarization of both transmitted and reflected wave to rotate. As a consequence, both the outgoing transmitted and reflected waves exhibit elliptical polarization. The major axis of the ellipse is rotated relatively to the original polarization direction. The real part of the rotation angle describes the change in polarization for linearly polarized light, while the imaginary part indicates the ellipticity of the transmitted or reflected light.

The complex rotational parameters characterizing the transmitted light can be expressed in terms of transmission amplitudes by

$$\theta_2^T + i\theta_1^T = \frac{1}{2}\ln\frac{t_+(\omega)}{t_-(\omega)}, \tag{8}$$

where $t_\pm$ represent the transmission amplitudes of transmitted electric fields. In the case of a weak magnetic field ($g \ll 1$), a perturbation expansion can be applied. The leading-order contribution can be obtained by expanding $t_\pm$ around the refractive index of the slab in the absence of the magnetic field $\boldsymbol{B}$:

$$\theta_2^T + i\theta_1^T = \frac{g}{2n}\frac{\partial \ln[t(\omega)]}{\partial n}, \tag{9}$$

where $n = \sqrt{\epsilon}$ represents the refractive index of the slab. Similarly, the leading-order expressions of complex angles of the Kerr rotation, in the case of a weak magnetic field, are given by

$$\theta_2^{R^{(l/r)}} + i\theta_1^{R^{(l/r)}} = \frac{g}{2n}\frac{\partial \ln[r^{(l/r)}(\omega)]}{\partial n}, \tag{10}$$

where $r^{(l/r)}$ is the left/right reflection amplitudes in the absence of magnetic field $\boldsymbol{B}$.

$\mathcal{PT}$ symmetry constraints on scattering amplitudes. The $\mathcal{PT}$ symmetry can be implemented in quantum tunneling time and magneto-optic effects by imposing conditions on the interaction potential in the Schrödinger equation and on dielectric permittivity in eq. (6): $V(x) = V^*(-x)$. As discussed in ref. [25], the parametrization of the scattering matrix only requires three independent real functions in a $\mathcal{PT}$-symmetric system: one inelasticity, $\eta \in [1, \infty]$, and two phase shifts, $\delta_{1,2}$. In terms of η and $\delta_{1,2}$, the transmission and reflection amplitudes are given by

$$\begin{aligned} t &= \eta\frac{e^{2i\delta_1} + e^{2i\delta_2}}{2}, \\ r^{(r/l)} &= \eta\frac{e^{2i\delta_1} - e^{2i\delta_2}}{2} \pm i\sqrt{\eta^2 - 1}e^{i(\delta_1+\delta_2)}. \end{aligned} \tag{11}$$

As the consequence of $\mathcal{PT}$ symmetry constraints, two components of the traversal time are also given in terms of η and $\delta_{1,2}$ by

$$\begin{aligned} \tau_1 &= \frac{\mathrm{d}(\delta_1+\delta_2)}{\mathrm{d}E} + \eta\frac{\sin(2\delta_1) - \sin(2\delta_2)}{4E}, \\ \tau_2 &= \frac{\mathrm{d}\ln[\eta\cos(\delta_1-\delta_2)]}{\mathrm{d}E} + \eta\frac{\cos^2\delta_1 - \cos^2\delta_2}{2E}. \end{aligned} \tag{12}$$

Only three FR and KR angles are independent, the FR and KR angles are given in terms of η and $\delta_{1,2}$ by

$$\begin{aligned} \theta_1^T = \theta_1^R = \frac{g}{2n}\frac{\partial(\delta_1+\delta_2)}{\partial n}, \quad \theta_2^T = \frac{g}{2n}\frac{\partial \ln[\eta\cos(\delta_1-\delta_2)]}{\partial n}, \\ \theta_2^{R^{(r/l)}} = \frac{g}{2n}\frac{\partial}{\partial n}\ln|\eta\sin(\delta_1-\delta_2) \pm \sqrt{\eta^2-1}|. \end{aligned} \tag{13}$$

$\theta_2^{R^{(r/l)}}$ and θ_2^T are related by $\theta_2^{R^{(r)}} + \theta_2^{R^{(l)}} = \frac{2T}{T-1}\theta_2^T$, where $T = \eta^2\cos^2(\delta_1 - \delta_2)$ denotes the transmission coefficient.

A simple exact solvable $\mathcal{PT}$-symmetric model. – A simple $\mathcal{PT}$-symmetric contact interaction potential model is adopted in this letter to illustrate some usual features in both tunneling time and magneto-optic effects in $\mathcal{PT}$-symmetric systems. The $\mathcal{PT}$-symmetric interaction potential for a single cell of the barrier is chosen as

$$\begin{aligned} V(x) &= V\delta\left(x + \frac{L}{2}\right) + V^*\delta\left(x - \frac{L}{2}\right), \\ V &= |V|e^{i\varphi_V} = V_1 + iV_2, \end{aligned} \tag{14}$$

which represents two complex-conjugate impurities placed inside of a single cell. One is absorbing with loss and the other is emissive with an equal amount of gain. The closed forms of scattering solutions can be obtained for the contact interaction potential model:

i) Transmission and reflection amplitudes for a quantum particle tunneling through a single cell of the barrier of length Λ ($\Lambda = L + L_0$) are given by

$$t_0(k) = \frac{\csc(kL)e^{ikL_0}}{\mathcal{R}(k) - i\mathcal{I}(k)}, \quad r_0^{(l/r)}(k) = i\frac{Q^{(l/r)}(k)e^{ikL_0}}{\mathcal{R}(k) - i\mathcal{I}(k)}, \tag{15}$$

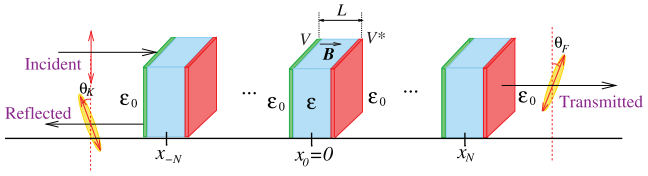

Fig. 2: Schematic of a one-dimension multiple cells $\mathcal{PT}$-symmetric photonic heterostructure.

where L_0 stands for the separation between two slabs, and

$$\mathcal{R}(k) = \cot(kL) + 2\frac{m|V|\cos\varphi_V}{k},$$
$$\mathcal{I}(k) = 1 - 2\left(\frac{m|V|}{k}\right)^2 - 2\left(\frac{m|V|\cos\varphi_V}{k}\right)\cot(kL),$$
$$Q^{(l/r)}(k) = -2\frac{m|V|}{k}\left[\frac{\cos(kL \mp \varphi_V)}{\sin(kL)} + \frac{m|V|}{k}\right]. \quad (16)$$

ii) The transmission and reflection amplitudes in eq. (15) also apply in the case of Faraday and Kerr effects for a single cell with slab of length Λ by replacing k by $\frac{\omega n}{c}$. The expression of functions $\mathcal{R}(\omega)$, $\mathcal{I}(\omega)$ and $Q^{(r/l)}(\omega)$ are given in eq. (15) and eq. (18) in ref. [28].

Periodic multiple cells $\mathcal{PT}$-symmetric systems. It is known that when the wave propagation through a medium is described by a differential equation of second order, the expression for the total transmission from the finite periodic system for any waves (sound and electromagnetic) depends on the unit cell transmission, the Bloch phase and the total number of cells. The infinite periodic $\mathcal{PT}$-symmetric structures exhibit unusual properties, including the band structure, Bloch oscillations, unidirectional propagation and enhanced sensitivity, see, *e.g.*, refs. [37–40] and references therein. However, the case of scattering in a finite periodic system composed of an arbitrary number of cells/scatters has been less investigated, despite the fact that any open quantum system generally consists of a finite system coupled with an infinite environment. In Hermitian theory, the averaged physical observables of a finite system approach the limit that depends on the crystal-momentum of an infinite periodic system as the size of a finite system is increased. However, in $\mathcal{PT}$-symmetric systems, new challenges emerge, the large size limit of a finite size system is only well-defined conditionally.

The $\mathcal{PT}$-periodic symmetric structure that consists of $2N+1$ cells, see fig. 2, can be assembled on top of a single cell. Following refs. [27,28,41], generic expressions for the transmission and reflection amplitudes for $2N+1$ cells of $\mathcal{PT}$-periodic symmetric structure in both tunneling time and magneto-optic effects cases can be presented as

$$t = \frac{1}{\cos(\beta(2N+1)\Lambda) + i\mathrm{Im}[\frac{1}{t_0}]\frac{\sin(\beta(2N+1)\Lambda)}{\sin(\beta\Lambda)}},$$
$$\frac{r^{(l/r)}}{t} = \frac{r_0^{(l/r)}}{t_0}\frac{\sin(\beta(2N+1)\Lambda)}{\sin(\beta\Lambda)}. \quad (17)$$

β plays the role of crystal-momentum for a periodic lattice and is related to k or ω by

$$\cos(\beta\Lambda) = Re\left[\frac{1}{t_0}\right]. \quad (18)$$

The factor $\frac{\sin(\beta(2N+1)\Lambda)}{\sin(\beta\Lambda)}$ in both transmission and reflection amplitudes reflects the combined interference and diffraction effects in finite periodic systems, which occur naturally in Hermitian one-dimensional finite-size periodic systems. It is interesting to see that eq. (17) holds up for both Hermitian and $\mathcal{PT}$-symmetric systems, which is highly non-trivial since the usual probability conservation property for Hermitian systems must be generalized in $\mathcal{PT}$-symmetric systems. As pointed out in ref. [27], the scattering amplitudes for a periodic multiple cells system can be related to single cell amplitudes in a compact fashion. This is ultimately due to the factorization of dynamics living in two distinct physical scales: short-range dynamics in a single cell and long-range collective effects of the periodic structure of the entire system. The short-range interaction dynamics is described by single cell scattering amplitudes and β represents the long-range correlation effect of the entire lattice system. The occurrence of factorization of short-range dynamics and long-range collective mode has been known in both condensed-matter physics and nuclear/hadron physics. As examples, particles interacting with short-range potential in a periodic box or trap, quantization conditions can be given in a compact formula that is known as Korringa-Kohn-Rostoker method [42,43] in condensed-matter physics, Lüscher formula [44] in lattice quantum chromodynamics and Busch-Englert-Rzażewski-Wilkens formula [45] in the nuclear-physics community. Other related useful discussions can be found in, *e.g.*, refs. [46–50].

Spectral singularities and their impact on tunneling time and magneto-optic effects in $\mathcal{PT}$-symmetric systems. Two types of singularities are present in scattering amplitudes: 1) a branch cut siting along the positive real axis in complex k- or ω-plane that separates physical sheet (the first Riemann sheet) and unphysical sheet (the second Riemann sheet); 2) poles of transmission and reflection amplitudes. These poles are called spectral singularities of a non-Hermitian Hamiltonian when they show up on the real axis [51–53], which yields divergences of reflection and transmission coefficients of scattered states.

The motion of poles in complex k- or ω-plane, fig. 3, has some profound impact on the value of τ_1 in tunneling time and Faraday and Kerr rotation angles θ_1^T and θ_1^R in $\mathcal{PT}$-symmetric systems. The location of these poles are model parameters dependent and can be found by solving $1/t = 0$. The normal or anomalous behaviours of τ_1 and $\theta_1^{T/R}$ are determined by the location of poles: when the poles are all located in an unphysical sheet (the second Riemann sheet), τ_1 and $\theta_1^{T/R}$ remains positive. As poles move close to and ultimately cross the real axis into the

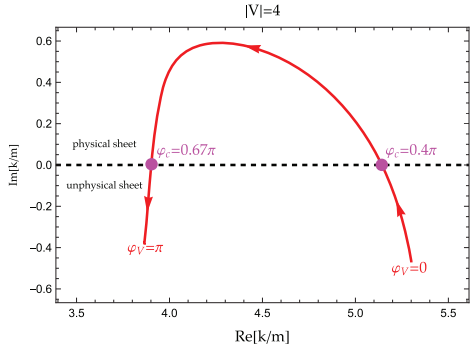

Fig. 3: The motion of poles in the complex k/m-plane as a function of increasing φ_V for tunneling time of a single cell defined in eq. (15) and eq. (16). The arrows indicate increasing φ_V directions. The φ_V values of spectral singularities are indicated by φ_c's. The model parameters are taken as $|V| = 4$ and $mL = 1$.

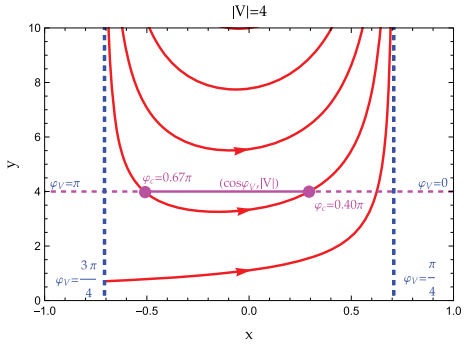

Fig. 4: Spectral singularities condition plot: the parametric plot of the solid red curve is generated with (x, y) coordinates given by the left-hand side of eq. (21) as a function of k/m. The solid red curve is bound by two blue vertical lines located at $x = \pm\frac{1}{\sqrt{2}}$. The purple line is generated with coordinates $(\cos\varphi_V, |V|)$ by varying φ_V in the range $[0, \pi]$. The arrows indicate increasing k/m directions. The spectral singularities for fixed $m|V|$ are given by the intersection of the purple line and the red curve. The model parameters are chosen as $|V| = 4$, and $mL = 1$.

physical sheet (the first Riemann sheet), the poles generate an enhancement in τ_1 and $\theta_1^{T/R}$ near the location of the poles. The spectral singularities occur when the poles are located on the real axis, the transmission and reflection amplitudes diverge at the location of the poles. This can be easily understood with the motion of a single pole. Near the pole, the transmission amplitude is approximated by

$$t(k) \propto \frac{1}{k - k_{pole}} = \frac{k - k_{re} - i\gamma}{(k - k_{re})^2 + \gamma^2}, \tag{19}$$

where $k_{pole} = k_{re} + i\gamma$, being k_{re} and γ the real and imaginary parts of pole position. The location of the pole in the physical sheet or unphysical sheet is determined by the sign of γ: unphysical sheet if $\gamma < 0$ and physical sheet if $\gamma > 0$. The tunneling time τ_1 or Faraday/Kerr rotation angle $\theta_1^{T/R}$ near the pole is thus dominated by

$$\tau_1 \sim \frac{m}{k} \frac{\gamma}{(k - k_{re})^2 + \gamma^2}, \tag{20}$$

hence as the pole moves across the real axis into the physical sheet, γ changes its sign.

The locations of the moving poles are controlled by model parameters. The spectral singularities only occur in a certain range of model parameters, the boundary of the range of the model parameters hence separates the normal behaviour of the tunneling time and Faraday/Kerr rotation angles where τ_1 and $\theta_1^{T/R}$ always remain positive from anomalous behaviours where τ_1 and $\theta_1^{T/R}$ may turn negative near location of the spectral singularities. When the model parameters are varied continuously, the tunneling time and Faraday/Kerr rotation angles in $\mathcal{PT}$-symmetric systems hence experience a phase-transition–like transformation. Using the expressions in eq. (15) and eq. (16) as a simple example, the conditions for spectral singularities are given by considering $1/t_0(k) = 0$:

$$\left(-\frac{\cot(kL)|\sin(kL)|}{\sqrt{2}}, \frac{k/m}{\sqrt{2}|\sin(kL)|} \right) = (\cos\varphi_V, |V|). \tag{21}$$

The solutions of the spectral singularities can be visualized graphically by observing the intersection of a curve and a line with (x, y) coordinates given by both sides of eq. (21) for a fixed $|V|$, see fig. 4 as an example. For a fixed $|V| = 4$, the solutions of the spectral singularities can only be found in a finite range, $\varphi_V \in [0.4\pi, 0.67\pi]$, in which the poles appear in the physical sheet, anomalous behaviour of tunneling time and Faraday/Kerr rotation angles occur and τ_1 and $\theta_1^{T/R}$ may turn negative. For a fixed $|V| = 4$, only a single pole solution can be found in the complex k-plane, the motion of pole as φ_V is increased is illustrated in fig. 3.

For a large-N system, the situation is even more interesting, the band structure and EPs start getting involved, competing with poles and playing the roles in turning τ_1 and $\theta_1^{T/R}$, see detailed discussion in ref. [27]. The band structure of the system is clearly visible for even small-size systems. The number of poles grows drastically with size, and the distribution of poles splits into bands. When the poles show up inside an allowed band of the system and all move across the real axis, they tend to flip the sign of the entire band. In some bands where two bands start merging together at an exceptional point, the exceptional points tend to force τ_1 and $\theta_1^{T/R}$ approaching zero and start to competing with poles, so the $\mathcal{PT}$-symmetric systems become almost transparent near EPs. The fate of τ_1 and $\theta_1^{T/R}$ near EPs now is the result of two competing forces: the poles and EPs.

Large-N limit. As the number of cells is increased, all traversal time $\tau_{1,2}$ and FR and KR angles demonstrate fast oscillating behaviour due to $\sin(\beta(2N + 1)\Lambda)$ and $\cos(\beta(2N + 1)\Lambda)$ functions in transmission and reflection amplitudes. For the large-N systems, we can introduce

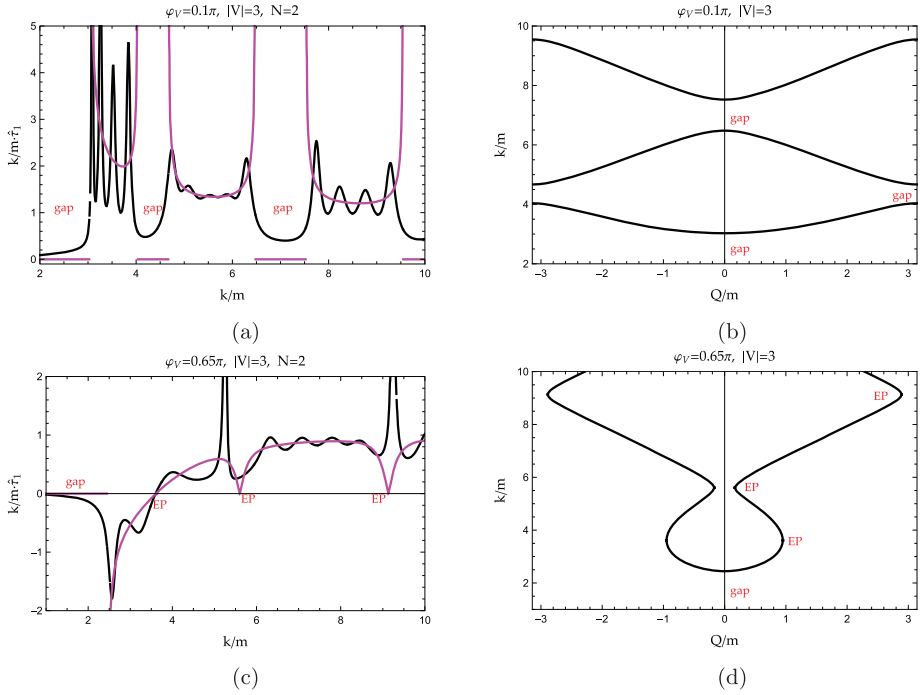

Fig. 5: (a) and (c): comparison of $\frac{k}{m}\hat{\tau}_1$ (solid black line) together with $\frac{k}{m}\frac{\mathrm{dRe}[Q]}{\mathrm{d}E}$ (solid purple/light grey line) in the unbroken and broken $\mathcal{PT}$-symmetric phase. (b) and (d): the corresponding band structure plot in the unbroken and broken $\mathcal{PT}$-symmetric phase. The rest of the parameters are taken as $mL = 1$ and $ma = 0.2$, where $|V|$ is dimensionless.

the traversal time per unit cell and FR and KR angles per unit cell, such as

$$\hat{\tau}_{1,2} = \frac{\tau_{1,2}}{(2N+1)\Lambda}. \tag{22}$$

The $N \to \infty$ limit may be approached by adding a small imaginary part to β: $\beta \to \beta + i\epsilon$, where $\epsilon \gg \frac{1}{(2N+1)\Lambda}$. As discussed in ref. [27], adding a small imaginary part to β is justified by considering the averaged FR and KR angles per unit cell, which ultimately smooth out the fast oscillating behaviour of $\tau_{1,2}$ and FR and KR angles. Therefore, as $N \to \infty$, the two components of traversal time per unit cell approach

$$\hat{\tau}_1 - i\hat{\tau}_2 \overset{N\to\infty}{\to} \frac{\mathrm{d}\beta}{\mathrm{d}E}, \tag{23}$$

and FR and KR angles per unit cell approach

$$\hat{\theta}_1^T - i\hat{\theta}_2^T \overset{N\to\infty}{\to} \frac{g}{2n}\frac{\partial\beta}{\partial n}, \qquad \hat{\theta}_2^{R^{(r/l)}} \overset{N\to\infty}{\to} 0. \tag{24}$$

The examples of tunneling time per unit cell for a $\mathcal{PT}$-symmetric finite system with five cells are shown in fig. 5, compared with the large-N limit results. As we can see in fig. 5, τ_1 oscillates around the large-N limit results. Even for the small-size system, we can see clearly that the band structure of infinite periodic system is already showing up. In the broken $\mathcal{PT}$-symmetric phase in fig. 5, EPs can be visualized even for a small-size system, where two neighbouring bands merge and the $\mathcal{PT}$ becomes totally transparent: τ_1 approaches zero. FR/KR angles show a similar behaviour, see, *e.g.*, fig. 4 and fig. 5 in ref. [28].

The limiting cases in eq. (23) and eq. (24) work well and are mathematically well defined in bands where spectral singularities are absent on the real axis, the poles are all either in the physical sheet or already all crossed real axis into the unphysical sheet. The large-N limit is well defined and can be achieved by either averaging fast oscillating behaviour of τ_E or using $i\epsilon$-prescription by shifting k off the real axis into the complex plane. However, in the bands where the divergent singularities show up on the real axis and the band is still in the middle of the transition between all positive and all negative bands of τ_1 and $\theta_1^{T/R}$, see, *e.g.*, fig. 8 in ref. [27], eq. (23) and eq. (24) break down, and the large-N limit becomes ambiguous and problematic. The question of how to define a physically meaningful large-N limit in the presence of spectral singularities is still open.

Summary. – We give a brief review on the recent development of the generalization of tunneling time and anomalous behaviour of the Faraday and Kerr rotation angles in $\mathcal{PT}$-symmetric systems. Both phenomena are closely related to each other, associated with a generalized density of states and exhibit a phase-transition–like anomalous behaviour in a certain range of model parameters. The anomalous behaviour of tunneling time and Faraday/Kerr angles in $\mathcal{PT}$-symmetric systems is directly related to the motion of poles of scattering amplitudes in the energy/frequency complex plane. When poles show up in physical sheets, the value of the tunneling time τ_1 and Faraday and Kerr rotation angles $\theta_1^{T/R}$ may turn

negative, which may be considered as an anomalous phase of $\mathcal{PT}$-symmetric systems. On the contrary, when all poles remain in the unphysical sheet, the tunneling time and Faraday/Kerr angles of $\mathcal{PT}$-symmetric systems behave just as normal Hermitian systems, which may be considered as normal phase of systems. Both τ_1 and $\theta_1^{T/R}$ exhibit a strong enhancement when the poles move close to the real axis where spectral singularities occur.

* * *

VG, AP-G and EJ would like to thank UPCT for partial financial support through "Maria Zambrano ayudas para la recualificación del sistema universitario español 2021–2023" financed by Spanish Ministry of Universities with funds "Next Generation" of EU. This research was supported in part by the National Science Foundation under Grant No. NSF PHY-1748958.

Data availability statement: The data that support the findings of this study are available upon reasonable request from the authors.

REFERENCES

[1] Ruschhaupt A., Delgado F. and Muga J. G., *J. Phys. A: Math. Gen.*, **38** (2005) L171.
[2] Yoshino T., *J. Opt. Soc. Am. B: Opt. Phys.*, **22** (2005) 1856.
[3] Zamani M., Ghanaatshoar M. and Alisafaee H., *J. Opt. Soc. Am. B: Opt. Phys.*, **28** (2011) 2637.
[4] Corzo N. V., Marino A. M., Jones K. M. and Lett P. D., *Phys. Rev. Lett.*, **109** (2012) 043602.
[5] Longhi S., *EPL*, **120** (2018) 64001.
[6] Muga J. G., *Phys. Today*, **57**, issue No. 2 (2004) 66.
[7] Mostafazadeh A., *J. Math. Phys.*, **43** (2002) 2814.
[8] Garmon S., Gianfreda M. and Hatano N., *Phys. Rev. A*, **92** (2015) 022125.
[9] Merkel A., Romero-García V., Groby J.-P., Li J. and Christensen J., *Phys. Rev. B*, **98** (2018) 201102.
[10] Zhu X., Ramezani H., Shi C., Zhu J. and Zhang X., *Phys. Rev. X*, **4** (2014) 031042.
[11] Lin Z., Ramezani H., Eichelkraut T., Kottos T., Cao H. and Christodoulides D. N., *Phys. Rev. Lett.*, **106** (2011) 213901.
[12] Feng L., Xu Y.-L., Fegadolli W. S., Lu M.-H., Oliveira J. E. B., Almeida V. R., Chen Y.-F. and Scherer A., *Nat. Mater.*, **12** (2013) 108.
[13] Landauer R. and Martin T., *Rev. Mod. Phys.*, **66** (1994) 217.
[14] Fayer M. and Fayer P., *Elements of Quantum Mechanics* (Oxford University Press) 2001.
[15] Gasparian V., Ortuño M., Schön G. and Simon U., in *Handbook of Nanostructured Materials and Nanotechnology* (Academic Press, San Diego) 2000.
[16] Büttiker M., Thomas H. and Prêtre A., *Z. Phys. B Condens. Matter*, **94** (1994) 133.
[17] Brouwer P. W., *Phys. Rev. B*, **58** (1998) R10135.
[18] Zhou F., Spivak B. and Altshuler B., *Phys. Rev. Lett.*, **82** (1999) 608.
[19] Muga J., Palao J., Navarro B. and Egusquiza I., *Phys. Rep.*, **395** (2004) 357.
[20] Birch K. P., *Opt. Commun.*, **43** (1982) 79.
[21] Stubkjaer K. E., *IEEE J. Sel. Top. Quantum Electron.*, **6** (2000) 1428.
[22] Wang Z., Chong Y. D., Joannopoulos J. D. and Soljačić M., *Phys. Rev. Lett.*, **100** (2008) 013905.
[23] Wang Z., Chong Y., Joannopoulos J. D. and Soljačić M., *Nature*, **461** (2009) 772.
[24] McGee N. W. E., Johnson M. T., de Vries J. J. and aan de Stegge J., *J. Appl. Phys.*, **73** (1993) 3418.
[25] Guo P. and Gasparian V., *Phys. Rev. Res.*, **4** (2022) 023083.
[26] Gasparian V., Guo P. and Jódar E., *Phys. Lett. A*, **453** (2022) 128473.
[27] Guo P., Gasparian V., Jódar E. and Wisehart C., *Phys. Rev. A*, **107** (2023) 032210.
[28] Perez-Garrido A., Guo P., Gasparian V. and Jódar E., *Phys. Rev. A*, **107** (2023) 053504.
[29] Gasparian V. and Pollak M., *Phys. Rev. B*, **47** (1993) 2038.
[30] Gasparian V., Ortuño M., Ruiz J., Cuevas E. and Pollak M., *Phys. Rev. B*, **51** (1995) 6743.
[31] Gasparian V., Christen T. and Büttiker M., *Phys. Rev. A*, **54** (1996) 4022.
[32] Wigner E. P., *Phys. Rev.*, **98** (1955) 145.
[33] Smith F. T., *Phys. Rev.*, **118** (1960) 349.
[34] Goldberger M. and Watson K., *Collision Theory*, *Dover Books on Physics* (Dover Publications) 2004.
[35] Lofy J., Gasparian V., Gevorkian Z. and Jódar E., *Rev. Adv. Mater. Sci.*, **59** (2020) 243.
[36] Gasparian V., Ortuño M., Ruiz J. and Cuevas E., *Phys. Rev. Lett.*, **75** (1995) 2312.
[37] Bender C. M., Dunne G. V. and Meisinger P. N., *Phys. Lett. A*, **252** (1999) 272.
[38] Shin K. C., *J. Phys. A: Math. Gen.*, **37** (2004) 8287.
[39] Musslimani Z. H., Makris K. G., El-Ganainy R. and Christodoulides D. N., *Phys. Rev. Lett.*, **100** (2008) 030402.
[40] Midya B., Roy B. and Roychoudhury R., *Phys. Lett. A*, **374** (2010) 2605.
[41] Gasparian V., Gummich U., Jódar E., Ruiz J. and Ortuño M., *Phys. B: Condens. Matter*, **233** (1997) 72.
[42] Korringa J., *Physica*, **13** (1947) 392.
[43] Kohn W. and Rostoker N., *Phys. Rev.*, **94** (1954) 1111.
[44] Lüscher M., *Nucl. Phys. B*, **354** (1991) 531.
[45] Busch T., Englert B.-G., Rzażewski K. and Wilkens M., *Found. Phys.*, **28** (1998) 549.
[46] Guo P. and Long B., *J. Phys. G: Nucl. Part. Phys.*, **49** (2022) 055104.
[47] Guo P. and Gasparian V., *Phys. Rev. D*, **103** (2021) 094520.
[48] Guo P. and Gasparian V., *J. Phys. A: Math. Theor.*, **55** (2022) 265201.
[49] Guo P., *Phys. Rev. C*, **103** (2021) 064611.
[50] Guo P. and Gasparian V., arXiv preprint, arXiv:2307.12951 (2023).
[51] Mostafazadeh A., *Phys. Rev. Lett.*, **102** (2009) 220402.
[52] Ahmed Z., *J. Phys. A: Math. Theor.*, **42** (2009) 472005.
[53] Longhi S., *Phys. Rev. B*, **80** (2009) 165125.